Conjugated Polymers

International Edition: DOI: 10.1002/anie.201911311
German Edition: DOI: 10.1002/ange.201911311

Controlling the Microstructure of Conjugated Polymers in High-Mobility Monolayer Transistors via the Dissolution Temperature

Mengmeng Li, Haijun Bin, Xuechen Jiao, Martijn M. Wienk, He Yan, and René A. J. Janssen**

Abstract: *It remains a challenge to precisely tailor the morphology of polymer monolayers to control charge transport. Herein, the effect of the dissolution temperature (T_{dis}) is investigated as a powerful strategy for morphology control. Low T_{dis} values cause extended polymer aggregation in solution and induce larger nanofibrils in a monolayer network with more pronounced π–π stacking. The field-effect mobility of the corresponding monolayer transistors is significantly enhanced by a factor of four compared to devices obtained from high T_{dis} with a value approaching 1 $cm^2 V^{-1} s^{-1}$. Besides that, the solution kinetics reveal a higher growth rate of aggregates at low T_{dis}, and filtration experiments further confirm that the dependence of the fibril width in monolayers on T_{dis} is consistent with the aggregate size in solution. The generalizability of the T_{dis} effect on polymer aggregation is demonstrated using three other conjugated polymer systems. These results open new avenues for the precise control of polymer aggregation for high-mobility monolayer transistors.*

Introduction

In organic field-effect transistors (OFETs), the few first monolayers of the organic semiconductor, either small molecules or conjugated polymers, at the interface with the insulator are of vital importance to the device performance due to their dominant role in transporting charges.[1] Therefore, downscaling organic semiconductors to a single molecular layer (monolayer) provides an ideal platform to investigate the intrinsic mechanism of charge transport. Considerable efforts have been made to realize high-performance organic-monolayer transistors from small molecules. For instance, field-effect mobilites of pentacene,[2] 2,7-dioctyl-[1]benzothieno[3,2-b][1]benzothiophene (C8-BTBT),[3] dicyanomethylene-substituted fused tetrathienoquinoid,[4] and 1,4-bis((5′-hexyl-2,2′-bithiophen-5-yl)ethynyl)benzene[5] have reached values on the order of 1–10 $cm^2 V^{-1} s^{-1}$ in monolayer transistors. In sharp contrast, monolayer transistors based on conjugated polymers generally exhibit mobilities that are orders of magnitude lower than their small-molecule counterparts, apart from few exceptions,[6] largely due to their lower crystallinity and associated challenges in controlling the morphology of the monolayer.

The aggregation behavior of conjugated polymers critically affects their film microstructure and subsequent performance in electronic devices. The microstructure can be affected via rational design of the chemical structure and control of the molecular weight or regioregularity.[7] It was found that planar conjugated backbones and high molecular weights are able to enhance intermolecular π–π stacking, contributing to stronger aggregation and longer conjugation lengths of the polymer chains. Another efficient strategy for tuning polymer aggregation is to tune the solvent quality.[8] For P(NDI2OD-T2), tolerably poor solvents resulted in elongated rod-like 300-nm aggregates in solution and enhanced field-effect mobility in thin films by a factor of 2.7.[8b] However, solvents with different qualities typically lead to a large variation of boiling points and vapor pressures, greatly limiting solution processing. For instance, the dip-coating technique, which allows the alignment of organic semiconductors with monolayer precision (2–3 nm), generally prefers solvents with lower boiling points, such as chloroform and dichloromethane.[9]

The degree of polymer aggregation can also be modulated by controlling the temperature of the solution from which films are cast. For conjugated polymers with extremely strong aggregation, a warm or even hot solution is required to achieve a homogeneous morphology.[7b,10] Although a modified dip-coating method operating at elevated temperatures

[*] Dr. M. Li
Key Laboratory of Microelectronic Devices and Integrated Technology, Institute of Microelectronics, Chinese Academy of Sciences
Beijing 100029 (China)
E-mail: limengmeng@ime.ac.cn

Dr. M. Li, Dr. H. Bin, Dr. M. M. Wienk, Prof. R. A. J. Janssen
Molecular Materials and Nanosystems, Institute for Complex Molecular Systems, Eindhoven University of Technology
P.O. Box 513, 5600 MB Eindhoven (The Netherlands)
E-mail: r.a.j.janssen@tue.nl

Dr. M. Li, Prof. R. A. J. Janssen
Dutch Institute For Fundamental Energy Research
De Zaale 20, 5612 AJ Eindhoven (The Netherlands)

Dr. X. Jiao
Australian Synchrotron, ANSTO
800 Blackburn Road, Clayton, Victoria 3168 (Australia),
and
Department of Materials Science and Engineering
Monash University
Wellington Road, Clayton, Victoria 3800 (Australia)

Prof. H. Yan
Department of Chemistry and Energy Institute
The Hong Kong University of Science and Technology
Clear Water Bay, Hong Kong (Hong Kong)

Supporting information and the ORCID identification number(s) for the author(s) of this article can be found under:
https://doi.org/10.1002/anie.201911311.

© 2019 The Authors. Published by Wiley-VCH Verlag GmbH & Co. KGaA. This is an open access article under the terms of the Creative Commons Attribution Non-Commercial License, which permits use, distribution and reproduction in any medium, provided the original work is properly cited, and is not used for commercial purposes.

was reported to tune the degree of polymer aggregation, the precision of thickness control is significantly reduced from 2–3 nm (one monolayer) to tens of nanometers due to the change of the solution viscosity and evaporation rate.[11]

In this contribution, a donor–acceptor-conjugated polymer with strong aggregation behavior, PffBT4T-2DT (Figure 1 a), is dissolved at various temperatures. It is found that at room temperature (RT), the peak in the UV/Vis–NIR absorption spectrum that corresponds to polymer aggregates is stronger and more pronounced when the polymer solution is prepared at a low dissolution temperature (T_{dis}). Furthermore, T_{dis} plays a critical role for the morphology of polymer monolayers obtained by dip-coating at RT. With decreasing T_{dis}, the fibril width in the polymer monolayer is almost doubled, resulting in a significant increase in field-effect mobility by a factor of 4. Particularly, at $T_{dis} = 55\,°C$, the saturated mobility of polymer-monolayer transistors approaches 1 $cm^2 V^{-1} s^{-1}$, which is among the best performances for polymer-monolayer transistors.[6a] The improved performance can be ascribed to the stronger π–π stacking interaction indicated by grazing-incidence wide-angle X-ray scattering (GIWAXS). The origin of the T_{dis} effect on polymer aggregation is explored by investigating the kinetics of aggregate growth and the dimension distribution of aggregates. It is demonstrated that a low T_{dis} leads to a higher growth rate and larger size of aggregates, facilitating the molecular order and subsequent charge transport. Importantly, the effect of T_{dis} on polymer aggregation appears to be a general phenomenon, as evidenced by studying three other conjugated polymers. As a result, T_{dis} provides a new, versatile parameter to precisely control polymer self-assembly and, consequently, to realize high-performance electronic devices.

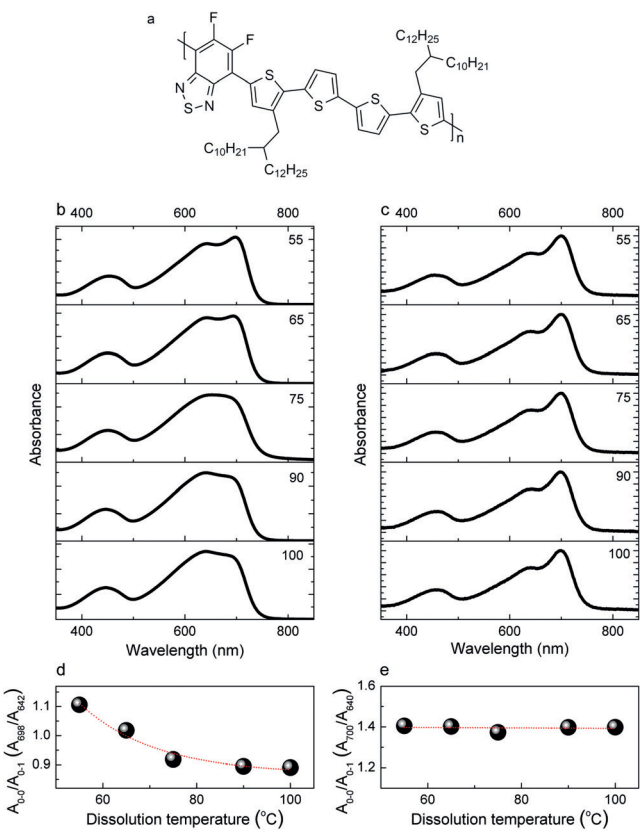

Figure 1. a) Structure of PffBT4T-2DT. b), c) UV/Vis–NIR absorption spectra of chloroform solutions (b) and polymer monolayers (c) recorded at RT. PffBT4T-2DT was dissolved at various temperatures (55, 65, 75, 90, and 100 °C). The polymer concentration in solution was 0.5 μM, and monolayers were dip-coated from a 0.5 $mg\,mL^{-1}$ chloroform solution with a speed of 100 $\mu m\,s^{-1}$. d), e) Corresponding absorbance ratio of the 0–0 to the 0–1 peak as a function of T_{dis}, fitted by red dashed lines, for (b) and (c), respectively.

Results and Discussion

In spite of its strong tendency to aggregate, PffBT4T-2DT can still be dissolved in chloroform with a polymer concentration of no less than 1 $mg\,mL^{-1}$ even at high molecular weight.[6a] It has to be emphasized that dissolved polymers will often exist in the form of solution-state supramolecular polymer aggregates.[12] The growth of these dissolved aggregates from a fully molecularly dissolved state has been explained by the disorder–order transition model[13] and multi-level self-assembly processes.[14] For conjugated polymers, the molecularly dissolved state is characterized by a single broad absorption peak in the UV/Vis–NIR absorption spectrum, while upon aggregation, a red-shift is observed due to planarization of the polymer backbone, accompanied by the appearance of vibronic peaks or shoulders.[13] Figure 1 b shows the RT UV/Vis–NIR absorption spectra of PffBT4T-2DT ($M_n = 48\,kg\,mol^{-1}$) solutions in chloroform, dissolved at various temperatures ranging from 55 to 100 °C. It is clearly visible that T_{dis} critically affects the aggregation behavior of PffBT4T-2DT in solution. For $T_{dis} = 55\,°C$, the absorption spectrum at RT is nearly identical to that in the solid state, where the intensity of 0–0 peak at 698 nm is larger than that of the 0–1 peak at 642 nm, which is indicative of J-aggregation.[15] In comparison, an increase in T_{dis} gradually reduces the intensity ratio of 0–0 to 0–1 peaks (A_{0-0}/A_{0-1}). At $T_{dis} > 65\,°C$, the A_{0-0}/A_{0-1} ratio drops below 1. When the polymer is dissolved at 100 °C, A_{0-0}/A_{0-1} is only 0.89 (Figure 1 d). It must be emphasized that the steady-state photoluminescence of the PffBT4T-2DT solution remains almost independent of T_{dis}, and time-resolved photoluminescence reveals similar lifetimes of around 1.4 ns (Figures S1 and S2 in the Supporting Information). Additionally, the impact of the cooling rate on polymer aggregation in solution is not discernible (Figures S3 and S4).

The optical properties of the polymer monolayers were also studied. The dip-coating technique that allows precise control of the film microstructure[6a,16] was employed to fabricate PffBT4T-2DT monolayers at RT from 0.5 $mg\,mL^{-1}$ chloroform solutions that were prepared at different T_{dis}. The optimized dip-coating speed is 100 $\mu m\,s^{-1}$. It is evident from Figure 1 c that at all T_{dis} values, the monolayers show strong J-aggregation with A_{0-0}/A_{0-1} up to 1.4. In comparison to the solution-absorption spectra, the film spectra are red-shifted by about 2 nm, suggesting a higher degree of molecular order and stronger π–π stacking interactions. Interestingly, T_{dis} has negligible influence on the UV/Vis–NIR spectra of the

 © 2020 The Authors. Published by Wiley-VCH Verlag GmbH & Co. KGaA, Weinheim

resulting polymer monolayers, as indicated by the red dashed line in Figure 1 e. Note that the change of $A_{0\text{–}0}/A_{0\text{–}1}$ in solution induced by T_{dis} is about 20% (Figure 1 d). The polymer aggregation/conjugation length is notably promoted during film formation due to solvent evaporation. Apparently, strong π–π stacking interactions between PffBT4T-2DT backbones in the solid films are capable of largely compensating the T_{dis} effect on polymer aggregation observed in solution.

To elucidate the impact of T_{dis} on the polymer monolayers in more detail, atomic force microscopy (AFM) in tapping mode was employed, and the corresponding surface topographies are shown in Figure 2. Heavily doped silicon wafers with 300 nm thermally grown SiO_2 were used as substrates. Figure 2 a shows that the thickness of the fibrillar ultrathin film is about 2.4 nm, which is defined as a single molecular layer because of its equivalence to the interlayer spacing of edge-on oriented multilayers,[6a] as will be discussed. Dip-coated at RT from solutions prepared at $T_{dis} = 55\,°C$, the fibril width of the resultant polymer monolayer is 74 ± 30 nm, in agreement with literature,[6a] and the corresponding height profile is presented in Figure 2 e. A small fraction of bright domains exists in the AFM height image (Figure 2 a), indicative of the starting growth of a second monolayer. When T_{dis} is increased, similar fibrillar microstructures are observed, but the second monolayer becomes less apparent (Figures 2 b,c,d and S5). However, more detailed analysis reveals the remarkable impact of T_{dis} on the fibril width. At $T_{dis} = 75\,°C$, the fibril width decreases by 35% with a value of 48 ± 14 nm, but further increase of T_{dis} to 90 or 100 °C only has minor effect on the fibril width (Figure 2 f). This trend of the fibril width as a function of T_{dis} is in excellent agreement with the solution-absorption spectra at various T_{dis} values (Figure 1 b,d). Therefore, it is concluded that the thinner nanofibers originate from decreased aggregation in solution at elevated T_{dis}.

The in-plane organization and qualitative orientational texture of the PffBT4T-2DT monolayer were probed by GIWAXS measurements. For the monolayers at $T_{dis} = 55\,°C$ (black curve in Figure 2 g), a distinct (010) π–π stacking peak is visible at $q = 1.74$ Å^{-1} in the in-plane profile, suggesting that the polymer chains are oriented in a pronounced edge-on fashion within the monolayer, with a π–π stacking distance of 0.36 nm. Note that the direct observation of a π–π stacking peak for a polymer monolayer has been rarely reported.[6b] Our results demonstrate that the PffBT4T-2DT monolayer prepared from a $T_{dis} = 55\,°C$ solution possesses a high degree of molecular order, which is attributed to the stronger aggregation in solution because of a lower T_{dis}. In sharp contrast, the reduced aggregation at a higher T_{dis} not only decreases the dimension of semi-crystalline fibrillar domains, that is, thinner nanofibers, but also noticeably influences the molecular order inside the nanofibers. It is evident that the (010) π–π stacking peak vanishes for the monolayer at $T_{dis} = 100\,°C$ (red curve in Figure 2 g and Figure S6), indicating that π–π interactions between polymer chains are significantly less pronounced.

The impact of T_{dis} on the polymer packing is further supported by PffBT4T-2DT drop-cast multilayers. In the out-of-plane GIWAXS profiles, strong lamellar (100), (200), (300), and even (400) peaks are visible for multilayers at $T_{dis} = 55$ and 90 °C (Figure S7), and a quantitative analysis reveals the same lamellar spacing of around 2.34 nm, in excellent agreement with the thickness of the PffBT4T-2DT monolayer (Figure 2 a–e). This result demonstrates the negligible impact of T_{dis} on the out-of-plane molecular organization for multilayers. On the contrary, the pronounced (010) peak is present

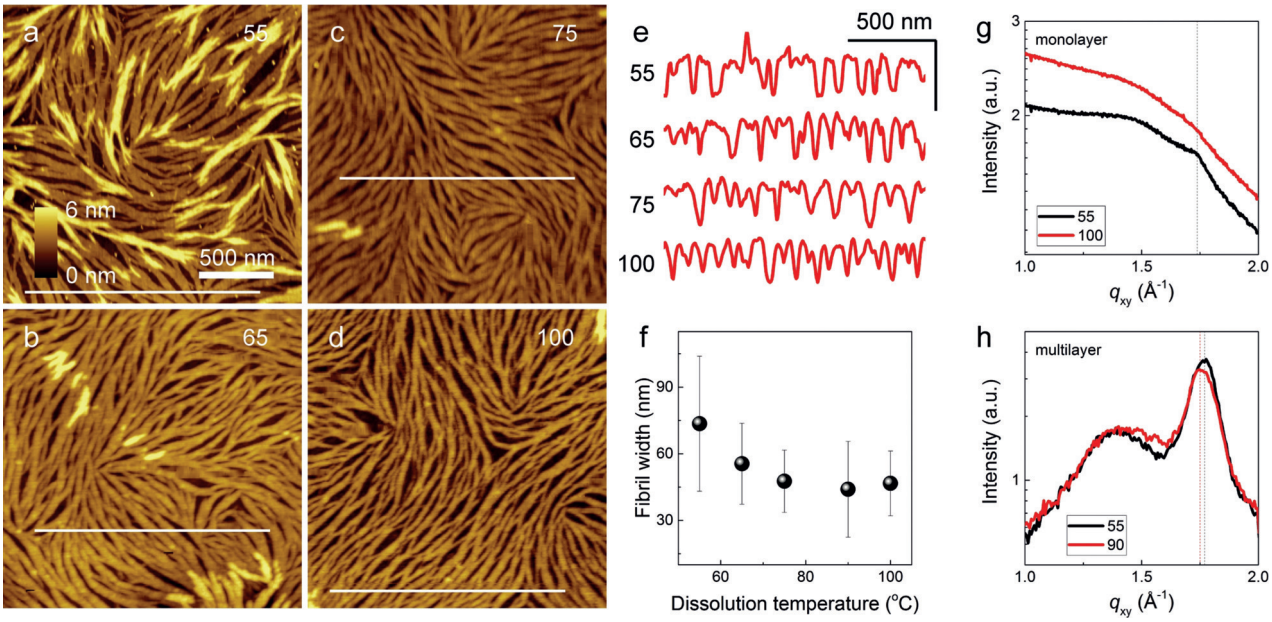

Figure 2. a)–d) AFM height images of PffBT4T-2DT monolayers dip-coated from solutions with different T_{dis} values. All AFM images have the same scale in *x*, *y*, and *z* direction. e) Corresponding height profiles of the white lines in (a)–(d). f) Fibril width as a function of T_{dis}. The average values and standard deviation for each sample are analyzed from over 100 fibers. g), h) GIWAXS in-plane profiles of a monolayer (g) and multilayer (h) with different T_{dis} values.

 © 2020 The Authors. Published by Wiley-VCH Verlag GmbH & Co. KGaA, Weinheim

in the in-plane profiles for both films, but the π-stacking distance decreases from 0.36 nm at $T_{dis}=90\,°C$ to 0.35 nm at $T_{dis}=55\,°C$ (Figure 2h). This closer polymer packing is consistent with the enhanced aggregation in solution at low T_{dis}.

To explore the relation between microstructure and charge transport for these polymer monolayers, field-effect transistors were fabricated with a bottom-gate bottom-contact configuration and SiO_2 as the dielectric. The same processing conditions were applied as for AFM. Prior to the polymer monolayer deposition, Au electrodes were patterned onto the Si/SiO_2 substrate, acting as source and drain electrodes, which were further modified by a 2,3,4,5,6-pentafluorothiophenol (PFBT) self-assembled monolayer (SAM) to minimize the contact resistance and to decrease the surface tension of the Au electrodes.[6a,17]

The transfer and output characteristics of the resultant polymer-monolayer transistors exhibit a typical linear/saturation behavior, and minor hysteresis is observed, as shown in Figure 3a,b. More importantly, the improvement of the device performance is achieved by applying a low T_{dis}. Starting from a gate voltage (V_{GS}) of 0 V, the drain current of the transistor obtained from $T_{dis}=55\,°C$ becomes higher than that obtained from $T_{dis}=100\,°C$. When increasing V_{GS} to −30 V, the drain-current difference roughly reaches one order of magnitude (Figure 3a). Extracted from the transfer curves, the saturated hole-mobilities (μ_h) are $0.87\pm0.04\,cm^2V^{-1}s^{-1}$ for $T_{dis}=55\,°C$ and $0.22\pm0.01\,cm^2V^{-1}s^{-1}$ for $T_{dis}=100\,°C$. The dependence of the saturated mobility on T_{dis} is plotted in Figure 3c. It seems that $T_{dis}=65\,°C$ is a threshold value after

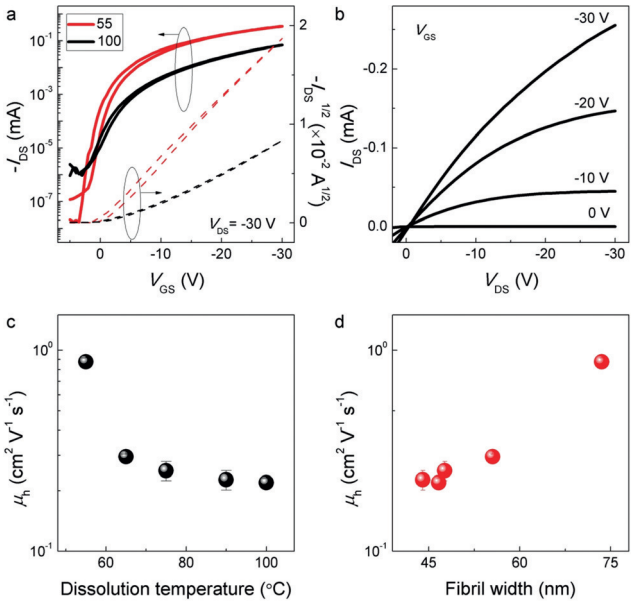

Figure 3. a) Transfer characteristics of PffBT4T-2DT monolayer transistors dip-coated from chloroform solutions with dissolution temperatures of 55 (red) and 100 °C (black). The drain voltage (V_{DS}) is −30 V. On-current (I_{on}) is defined as I_{DS} at $V_{GS}=-30$ V, and off-current (I_{off}) as I_{DS} at $V_{GS}=4$ V. b) Output characteristics of the PffBT4T-2DT monolayer transistor with a dissolution temperature of 55 °C. c), d) Saturated field-effect mobility (μ_h) as a function of dissolution temperature (c) and fibril width (d). The average value and error bar (standard deviation) for each condition are obtained from 10 devices.

which the mobility significantly drops by 66% (from $0.87\pm0.04\,cm^2V^{-1}s^{-1}$ to $0.30\pm0.01\,cm^2V^{-1}s^{-1}$). Above this T_{dis}, only a slight decrease in mobility is observed, with an average mobility of 0.22–0.30 $cm^2V^{-1}s^{-1}$. It is worth noting that this trend is similar with the fibril-width dependence on T_{dis}, and the relation between mobility and fibril width is plotted in Figure 3d. It is widely reported that a larger domain size is beneficial to the charge transport in OFET devices,[16] therefore, it is reasonable that thicker fibrillar domains contribute to higher mobility. Apparently, the fibril width over 60 nm is crucial for high-performance polymer monolayer transistors (Figure 3d). Additionally, the improvement of the device performance due to a low T_{dis} is also reflected in the threshold voltage (V_T) and on–off ratio (I_{on}/I_{off}): V_T gradually increases with T_{dis} (Figure S8) and I_{on}/I_{off} of the device obtained from $T_{dis}=55\,°C$ reaches 10^7, almost three orders of magnitude higher than that obtained from $T_{dis}=100\,°C$ (Figure 3a).

The mechanism of polymer aggregation in solution has been extensively investigated, and the disorder–order transition is one of the most accepted models.[13] In this model, starting from disordered polymer chains at high temperatures, polymer chains first planarize and then start to aggregate when the temperature of the solution is lowered. PffBT4T-2DT follows the expected trend with a more red-shifted and increasing aggregation peak in the UV/Vis–NIR absorption when the temperature of the solution decreases, as shown in Figure S9. To investigate the origin of the T_{dis} effect on the temperature-dependent aggregation of PffBT4T-2DT in more detail, UV/Vis–NIR absorption spectra were recorded for PffBT4T-2DT solutions prepared at different T_{dis} values (Figure S10). At the stage of planarization of the amorphous phase (≈60 °C, Figure S10a), a lower T_{dis} results in a small red-shift (≈5 nm) of the main absorption peak at around 600 nm, indicative of a more planar polymer backbone. When solutions are cooled to 55 °C (formation of the aggregated phase, Figure S10b), the T_{dis} effect on polymer aggregation is more pronounced, and larger red-shifts (≈15 nm) of the main absorption peak at 600 nm as well as an enhanced intensity of the aggregate peak at 696 nm can be seen for lower T_{dis}. These observations suggest that the lower T_{dis} not only facilitates the planarization of the polymer backbone but also generates more aggregates. For solutions at 40 °C (Figure S10c), further improvement of planarization or molecular order is obtained at low T_{dis}.

The polymer aggregation in solution can also be understood through a nucleation and growth process.[18] Therefore, the evolution of solution-absorption spectra with various T_{dis} values was studied, and the absorbance at 696 nm as a function of time is shown in Figure 4a. Quantitative analysis is conducted using the Avrami equation:[19]

$$\phi = 1-\exp(-k\,t^n) \tag{1}$$

where ϕ is the fraction of transformed aggregation at time t, n is the Avrami index, and k is the growth rate of the aggregation. Equation (1) can also be written in its logarithmic form:

$$\ln[-\ln(1-\phi)] = \ln k + n\ln t \tag{2}$$

 © 2020 The Authors. Published by Wiley-VCH Verlag GmbH & Co. KGaA, Weinheim

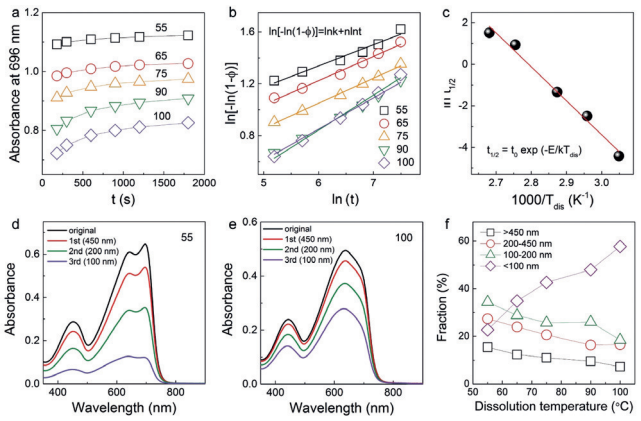

Figure 4. a) Evolution of absorbance at 696 nm with various T_{dis} values. PffBT4T-2DT is dissolved in chloroform (0.5 μM) on a hotplate at a certain temperature, and then cooled at RT starting at $t=0$ s. For each T_{dis}, the first absorption spectrum is recorded at $t=180$ s, at which time the solution is considered to have reached RT. b) Relation between the fraction of the transformed aggregation (ϕ) and evolution time (t) at various T_{dis} values. c) Dependence of the half-life ($t_{1/2}$) of the aggregation-growth procedure on T_{dis}. d), e) Absorption spectra after multiple filtration with $T_{dis}=55$ and 100 °C. f) Size distribution of dissolved aggregates as a function of T_{dis}.

Here, the value of ϕ can be estimated by A/A_{max}, where A is the absorbance at 696 nm at time t, and A_{max} the absorbance at 696 nm when the aggregation growth is complete. It is evident from Figure 4b that the Avrami equation describes the aggregation growth of PffBT4T-2DT very well. The corresponding parameters are listed in Table 1. $T_{dis}=55$ °C results in an almost threefold higher growth rate of aggregation compared to $T_{dis}=100$ °C, implying the generation of aggregated species with larger dimension.[18] Moreover, the half-life of this hypothetical aggregation growth process can be obtained from $t_{1/2}=[\ln(2)/k]^{1/n}$. It is interesting that the relation between $t_{1/2}$ and T_{dis} can be fitted by an Arrhenius equation:

Table 1: Avrami parameters of the polymer-aggregation growth at various T_{dis} values.

T_{dis} [°C]	55	65	75	90	100
k	1.43	1.11	0.90	0.55	0.46
n	0.16	0.19	0.19	0.24	0.27

$$t_{1/2} = t_0 \exp(-E/k_B\, T_{dis}) \tag{3}$$

where k_B is the Boltzmann constant and E is an apparent activation energy. $E=1.41$ eV is extracted from Figure 4c, further confirming that T_{dis} has a significant effect on the rate of polymer aggregation.

To test the effect of T_{dis} on the dimension of polymer aggregates that are in solution, attempted dynamic light scattering was employed but not successful due to absorption of PffBT4T-2DT in the range from 300 to 750 nm. Instead, the size of the aggregates is quantified by a three-cycle filtration experiment. To this end, chloroform solutions of PffBT4T-2DT were filtered sequentially using filters with pore sizes of 450, 200, and 100 nm, after which the corresponding UV/Vis–NIR absorption spectrum was recorded, as shown in Figures 4d,e and S11. The spectra reveal that after the three-cycle filtration, more aggregates are removed from solution at lower T_{dis} (purple spectra in Figure 4d,e). Quantitative analysis was carried out through spectrum integration in order to evaluate the size distribution of the aggregates (Figure 4f). With $T_{dis}=55$ °C, the aggregate fractions for <100 nm (purple diamonds), 100–200 nm (green triangles), 200–450 nm (red circles), and >450 nm (black squares) are 22.7 %, 34.4 %, 27.4 %, and 15.5 %, respectively. With increasing T_{dis}, the amount of aggregates over 100 nm gradually decreases, but more aggregates below 100 nm appear. Especially, when T_{dis} reaches up to 100 °C, the majority of polymer aggregates have a size of less than 100 nm. In all cases, the average size of the aggregates is roughly on the order of a few hundred nanometers, which seems larger than the value of the PffBT4T-2DT derivative PffBT4T-2OD, characterized by small-angle neutron scattering (≈ 40 nm).[20] It must be emphasized that the polymer aggregates tend to be reformed spontaneously after each filtration.[21] Therefore, care must be taken when using these fraction values extracted from filtration experiments. Nevertheless, the results demonstrate in a semi-quantitative way that a low T_{dis} is capable of sufficiently enhancing the polymer aggregation in solution, which is not only in excellent agreement with the solution absorption (Figure 1b) but also strongly supports the variations in fibril width, π–π stacking interactions, and field-effect mobility (Figures 2 and 3).

Several studies have emphasized that polymer aggregation and packing are largely dependent on the molecular weight.[7a,22] Therefore, two other batches of PffBT4T-2DT with lower molecular weights ($M_n=11$ and 18 kg mol^{-1}) were synthesized. Figure 5a reveals that the T_{dis} effect on the aggregation of the polymer decreases when lowering the molecular weight from 48 to 18 and then to 11 kg mol^{-1}. The concentration dependence was also investigated (Figure S12). The T_{dis} effect remains for polymer concentrations in the range of 0.5 to 50 μg mL^{-1}. From the data it is not possible to establish a quantitative relation between T_{dis} and the concentration of the polymer, but it is evident that at a fixed T_{dis}, the aggregation decreases for lower concentrations. The molecular weight and concentration-dependent results demonstrate that the intermolecular interaction between polymers plays a dominant role on polymer aggregation and modulate the T_{dis} effect.

To explore the generality of the T_{dis} effect, three other conjugated polymers P(NDI2OD-2T),[23] D-DPP3T-EH,[10c] and PffBT4T-2OD,[10b] all of which exhibit temperature-dependent aggregation behavior in chloroform, were studied (Figures 5b and S13). For P(NDI2OD-2T) and D-DPP3T-EH, the polymer aggregation is enhanced using lower T_{dis}, although the enhancement is smaller than for PffBT4T-2DT. Due to the lower solubility of PffBT4T-2OD compared to PffBT4T-2DT, a higher T_{dis} with a minimum value of 80 °C is required to dissolve PffBT4T-2OD, but the T_{dis} effect is otherwise identical to that of PffBT4T-2DT.

 © 2020 The Authors. Published by Wiley-VCH Verlag GmbH & Co. KGaA, Weinheim

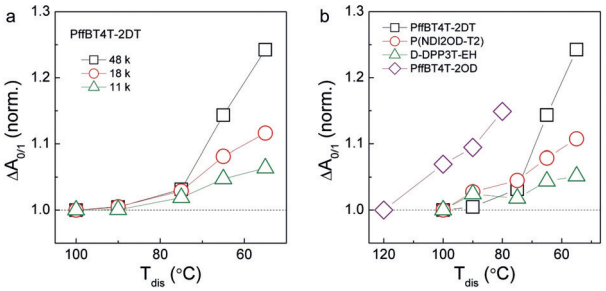

Figure 5. a) T_{dis} effect on polymer aggregation of PffBT4T-2DT as a function of molecular weight. b) Generalizability of the T_{dis} effect on polymer aggregation by characterizing three other conjugated polymers in chloroform. $A_{0/1} = A_{0\text{-}0}/A_{0\text{-}1}$, and $\Delta A_{0/1} = A_{0/1}(T)/A_{0/1}(100\,°C)$, where $A_{0/1}(T)$ and $A_{0/1}(100\,°C)$ are the $A_{0/1}$ values for solutions prepared at a certain temperature T and 100 °C, respectively. For PffBT4T-2OD, $\Delta A_{0/1} = A_{0/1}(T)/A_{0/1}(120\,°C)$.

Conclusion

In conclusion, a new strategy for the precise morphology control of polymer monolayers is proposed through tuning T_{dis}. It is confirmed by UV/Vis–NIR absorption that low T_{dis} values result in stronger polymer aggregation in solution, with more extended π–π stacking interactions and longer conjugation length. The T_{dis} effect on polymer aggregation is also observed for dip-coated polymer monolayers. With decreasing T_{dis}, the width of monolayer fibrils in the monolayer network is significantly increased, leading to improved polymer packing, as evidenced by AFM and GIWAXS. Importantly, the improved molecular order due to low T_{dis} boosts the charge transport with the mobility approaching $1\,cm^2\,V^{-1}\,s^{-1}$. The origin of this T_{dis} effect on polymer aggregation was explored. The growth rate of aggregates at low T_{dis} values is almost threefold higher compared to high T_{dis}, and the relation between the half-life of aggregation growth and T_{dis} can be well fitted by the Arrhenius equation. The generalizability of the T_{dis} effect is confirmed by investigating three other conjugated polymers. The results demonstrate that controlling the dissolution temperature of aggregated conjugated polymers is a new and interesting way to control polymer microstructures and enables to achieve high-performance electronic devices, as shown here for polymer-monolayer transistors.

Acknowledgements

The authors thank Dr. Junyu Li at DSM DMSC R&D Solutions for the GIWAXS measurements and discussion. This research was also undertaken on the SAXS/WAXS beamline at the Australian Synchrotron, part of ANSTO. It has received funding from the Netherlands Organisation for Scientific Research (016.Veni.192.106 and the NWO Spinoza prize awarded to R.A.J.J.) and from the Thousand Youth Talents Plan. We further acknowledge funding from the Ministry of Education, Culture and Science (Gravity program 024.001.035).

Conflict of interest

The authors declare no conflict of interest.

Keywords: aggregation · conjugated polymers · dissolution · fibrillar structure · monolayer transistors

How to cite: *Angew. Chem. Int. Ed.* **2020**, *59*, 846–852
Angew. Chem. **2020**, *132*, 856–862

[1] F. Dinelli, M. Murgia, P. Levy, M. Cavallini, F. Biscarini, D. M. de Leeuw, *Phys. Rev. Lett.* **2004**, *92*, 116802.
[2] Y. Zhang, J. Qiao, S. Gao, F. Hu, D. He, B. Wu, Z. Yang, B. Xu, Y. Li, Y. Shi, W. Ji, P. Wang, X. Wang, M. Xiao, H. Xu, J.-B. Xu, X. Wang, *Phys. Rev. Lett.* **2016**, *116*, 016602.
[3] D. He, J. Qiao, L. Zhang, J. Wang, T. Lan, J. Qian, Y. Li, Y. Shi, Y. Chai, W. Lan, L. K. Ono, Y. Qi, J.-B. Xu, W. Ji, X. Wang, *Sci. Adv.* **2017**, *3*, e1701186.
[4] Y. Shi, L. Jiang, J. Liu, Z. Tu, Y. Hu, Q. Wu, Y. Yi, E. Gann, C. R. McNeill, H. Li, W. Hu, D. Zhu, H. Sirringhaus, *Nat. Commun.* **2018**, *9*, 2933.
[5] L. Jiang, H. Dong, Q. Meng, H. Li, M. He, Z. Wei, Y. He, W. Hu, *Adv. Mater.* **2011**, *23*, 2059–2063.
[6] a) M. Li, D. K. Mangalore, J. Zhao, J. H. Carpenter, H. Yan, H. Ade, H. Yan, K. Müllen, P. W. M. Blom, W. Pisula, D. M. de Leeuw, K. Asadi, *Nat. Commun.* **2018**, *9*, 451; b) Z.-F. Yao, Y.-Q. Zheng, Q.-Y. Li, T. Lei, S. Zhang, L. Zou, H.-Y. Liu, J.-H. Dou, Y. Lu, J.-Y. Wang, X. Gu, J. Pei, *Adv. Mater.* **2019**, *31*, 1806747.
[7] a) M. Li, C. An, W. Pisula, K. Müllen, *Acc. Chem. Res.* **2018**, *51*, 1196–1205; b) H. Hu, P. C. Y. Chow, G. Zhang, T. Ma, J. Liu, G. Yang, H. Yan, *Acc. Chem. Res.* **2017**, *50*, 2519–2528; c) R. Steyrleuthner, R. Di Pietro, B. A. Collins, F. Polzer, S. Himmelberger, M. Schubert, Z. Chen, S. Zhang, A. Salleo, H. Ade, A. Facchetti, D. Neher, *J. Am. Chem. Soc.* **2014**, *136*, 4245–4256; d) M. Li, A. H. Balawi, P. J. Leenaers, L. Ning, G. H. L. Heintges, T. Marszalek, W. Pisula, M. M. Wienk, S. C. J. Meskers, Y. Yi, F. Laquai, R. A. J. Janssen, *Nat. Commun.* **2019**, *10*, 2867.
[8] a) M. Li, C. An, T. Marszalek, M. Baumgarten, H. Yan, K. Müllen, W. Pisula, *Adv. Mater.* **2016**, *28*, 9430–9438; b) M. M. Nahid, A. Welford, E. Gann, L. Thomsen, K. P. Sharma, C. R. McNeill, *Adv. Electron. Mater.* **2018**, *4*, 1700559.
[9] a) W. Wang, L. Wang, G. Dai, W. Deng, X. Zhang, J. Jie, X. Zhang, *Nano-Micro Lett.* **2017**, *9*, 52; b) J. Jang, S. Nam, K. Im, J. Hur, S. N. Cha, J. Kim, H. B. Son, H. Suh, M. A. Loth, J. E. Anthony, J.-J. Park, C. E. Park, J. M. Kim, K. Kim, *Adv. Funct. Mater.* **2012**, *22*, 1005–1014.
[10] a) Z. Chen, P. Cai, J. Chen, X. Liu, L. Zhang, L. Lan, J. Peng, Y. Ma, Y. Cao, *Adv. Mater.* **2014**, *26*, 2586–2591; b) Y. Liu, J. Zhao, Z. Li, C. Mu, W. Ma, H. Hu, K. Jiang, H. Lin, H. Ade, H. Yan, *Nat. Commun.* **2014**, *5*, 5293; c) G. H. L. Heintges, P. J. Leenaers, R. A. J. Janssen, *J. Mater. Chem. A* **2017**, *5*, 13748–13756.
[11] G. Ouyang, H. Wu, X. Qiao, J. Zhang, H. Li, *ACS Omega* **2018**, *3*, 9290–9295.
[12] a) Y.-Q. Zheng, Z.-F. Yao, T. Lei, J.-H. Dou, C.-Y. Yang, L. Zou, X. Meng, W. Ma, J.-Y. Wang, J. Pei, *Adv. Mater.* **2017**, *29*, 1701072; b) D. R. Reid, N. E. Jackson, A. J. Bourque, C. R. Snyder, R. L. Jones, J. J. de Pablo, *J. Phys. Chem. Lett.* **2018**, *9*, 4802–4807; c) Y. Xi, C. M. Wolf, L. D. Pozzo, *Soft Matter* **2019**, *15*, 1799–1812.
[13] a) F. Panzer, H. Bässler, A. Köhler, *J. Phys. Chem. Lett.* **2017**, *8*, 114–125; b) A. Köhler, S. T. Hoffmann, H. Bässler, *J. Am. Chem. Soc.* **2012**, *134*, 11594–11601; c) B. M. W. Langeveld-

 © 2020 The Authors. Published by Wiley-VCH Verlag GmbH & Co. KGaA, Weinheim

Voss, M. P. T. Christiaans, R. A. J. Janssen, E. W. Meijer, *Macromolecules* **1998**, *31*, 6702 – 6704.
[14] Z.-F. Yao, Y.-Q. Zheng, Q.-Y. Li, T. Lei, S. Zhang, L. Zou, H.-Y. Liu, J.-H. Dou, Y. Lu, J.-Y. Wang, X. Gu, J. Pei, *Adv. Mater.* **2019**, *31*, 1806747.
[15] F. C. Spano, *Acc. Chem. Res.* **2010**, *43*, 429 – 439.
[16] a) M. Li, C. An, T. Marszalek, M. Baumgarten, K. Müllen, W. Pisula, *Adv. Mater.* **2016**, *28*, 2245 – 2252; b) M. Li, T. Marszalek, Y. Zheng, I. Lieberwirth, K. Müllen, W. Pisula, *ACS Nano* **2016**, *10*, 4268 – 4273.
[17] D. J. Gundlach, J. E. Royer, S. K. Park, S. Subramanian, O. D. Jurchescu, B. H. Hamadani, A. J. Moad, R. J. Kline, L. C. Teague, O. Kirillov, C. A. Richter, J. G. Kushmerick, L. J. Richter, S. R. Parkin, T. N. Jackson, J. E. Anthony, *Nat. Mater.* **2008**, *7*, 216.
[18] N. E. Persson, P.-H. Chu, M. McBride, M. Grover, E. Reichmanis, *Acc. Chem. Res.* **2017**, *50*, 932 – 942.
[19] a) M. Avrami, *J. Chem. Phys.* **1939**, *7*, 1103 – 1112; b) M. Avrami, *J. Chem. Phys.* **1940**, *8*, 212 – 224.
[20] Z. Bi, H. B. Naveed, Y. Mao, H. Yan, W. Ma, *Macromolecules* **2018**, *51*, 6682 – 6691.
[21] H.-L. Yi, C.-C. Hua, *Macromolecules* **2019**, *52*, 332 – 340.
[22] T. Marszalek, M. Li, W. Pisula, *Chem. Commun.* **2016**, *52*, 10938 – 10947.
[23] R. Steyrleuthner, M. Schubert, I. Howard, B. Klaumünzer, K. Schilling, Z. Chen, P. Saalfrank, F. Laquai, A. Facchetti, D. Neher, *J. Am. Chem. Soc.* **2012**, *134*, 18303 – 18317.

Manuscript received: September 4, 2019
Revised manuscript received: October 13, 2019
Version of record online: November 20, 2019

 © 2020 The Authors. Published by Wiley-VCH Verlag GmbH & Co. KGaA, Weinheim